

New dinuclear macrocyclic copper(II) complexes as potentially fluorescent and magnetic materials

Table of contents:

Figure S1. IR spectrum of **K1**.

Figure S2. IR spectrum of **K2**.

Figure S3. a) TG-DTA traces of **K1** and b) **K2**.

Figure S4. a) TG-DTA traces of **K1** and b) IR spectra decomposition products.

Figure S5. a) TG-DTA traces of **K2** and b) IR spectra decomposition products.

Figure S6. XRD of the thermal analysis residue of **K1**.

Figure S7. XRD of the thermal analysis residue of **K2**.

Figure S8. Powder EPR spectra recorded for **K1** (A) and **K2** (B) at 77 K.

Figure S9. Powder EPR spectra recorded for **K1** and **K2** at 350 K.

Figure S10. SEM/EDX images of **K1** mapping scanning size 300 μm .

Figure S11. SEM/EDX images of **K2** mapping scanning size 300 μm .

Figure S12. AFM of **K1/Si**, thermal deposition, scan size 5 μm , $R_a=4.02 \text{ nm}$, $R_q=5.36 \text{ nm}$.

Figure 13. IR DRIFT of **K1/Si** and **K2/Si** materials- thermal vapour deposition.

Table S1. The theoretical values of the $J(\text{Cu}_1\text{-Cu}_2)$ magnetic coupling constants [cm^{-1}], estimated within the broken-symmetry and spin-flip approach with B3LYP functional and def2-SVP/def2-QZVPP(Cu) basis set according to the three schemes: spin-projected (SP), spin-unprojected (SUP) and approximate spin-projected (AP).

Table S2. Relevant photophysical data of studied compounds: $\bar{\epsilon}_{\text{em}}$, $\bar{\epsilon}_{\text{ex}}$ [nm] $B_p=8$; λ [nm] (ϵ [$\text{dm}^3 \text{ mol}^{-1} \text{ cm}^{-1}$]); Stoke shift [nm], [cm^{-1}]; Q $B_p=5$.

Table S3. Fluorescence data of the thin materials **K1/Si** and **K2/Si** obtained by thermal vapour deposition.

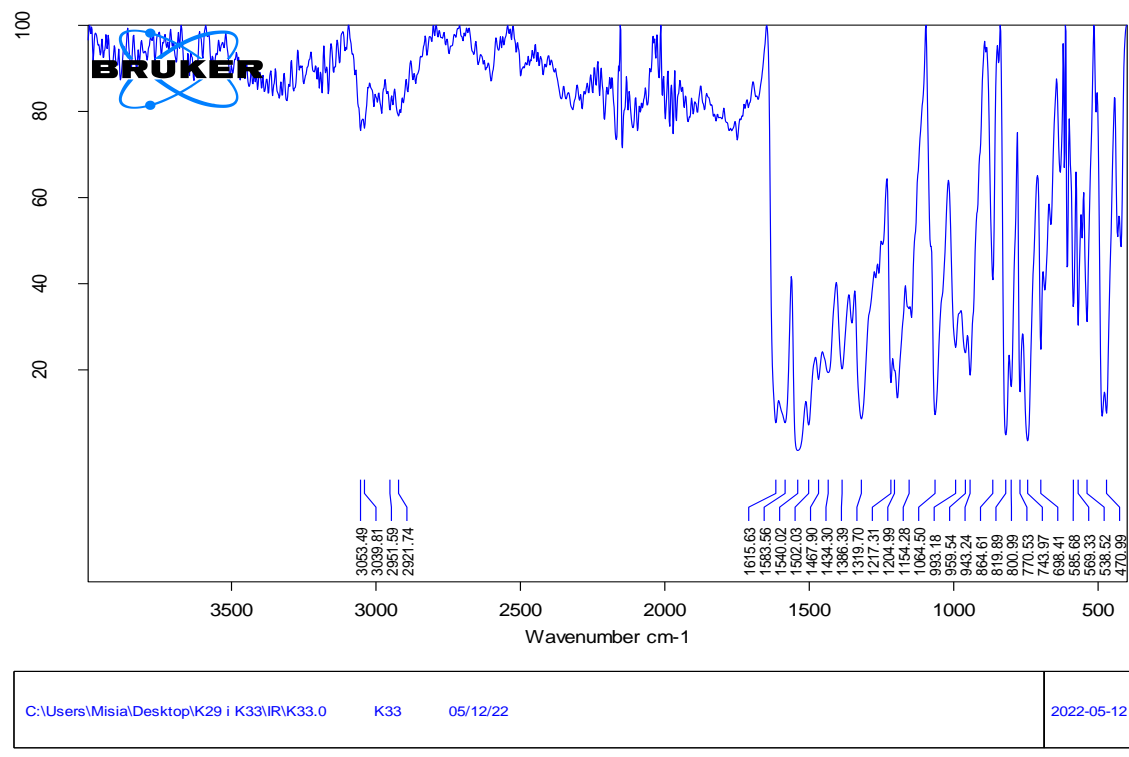


Figure S1. IR spectrum of **K1**.

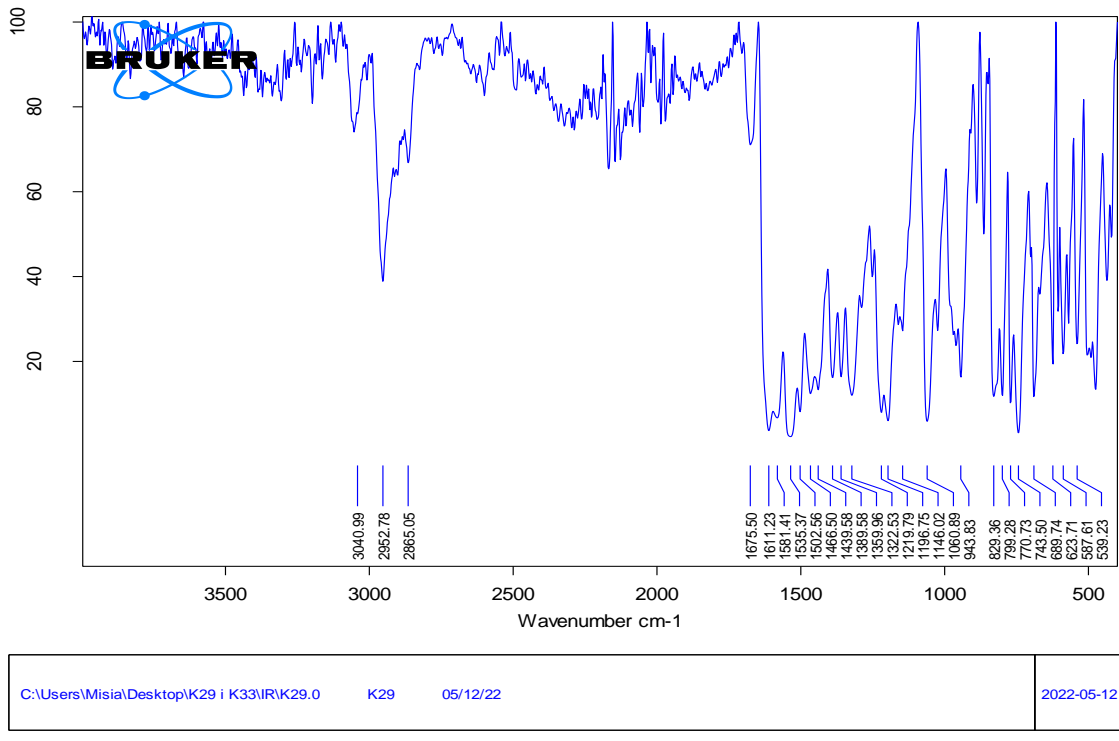


Figure S2. IR spectrum of K2.

Thermal analysis

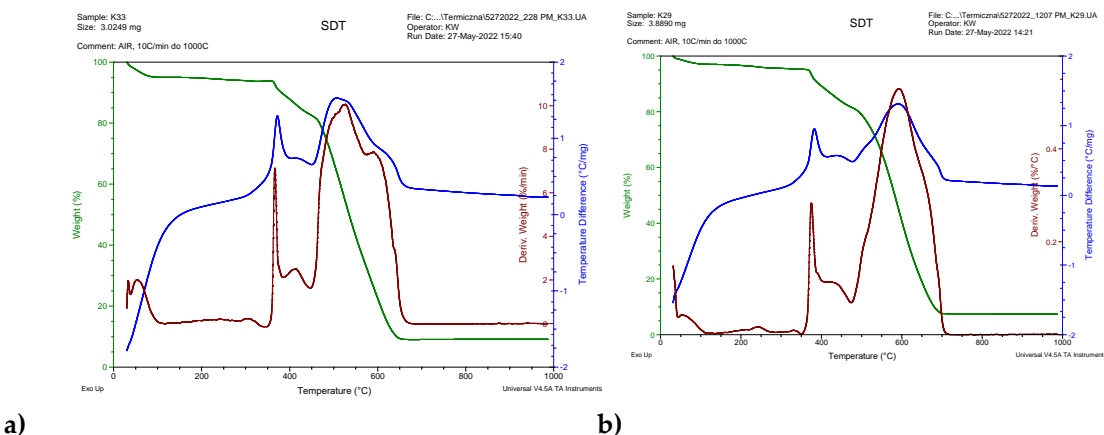


Figure S3. a) TG-DTA traces of K1 and b) K2.

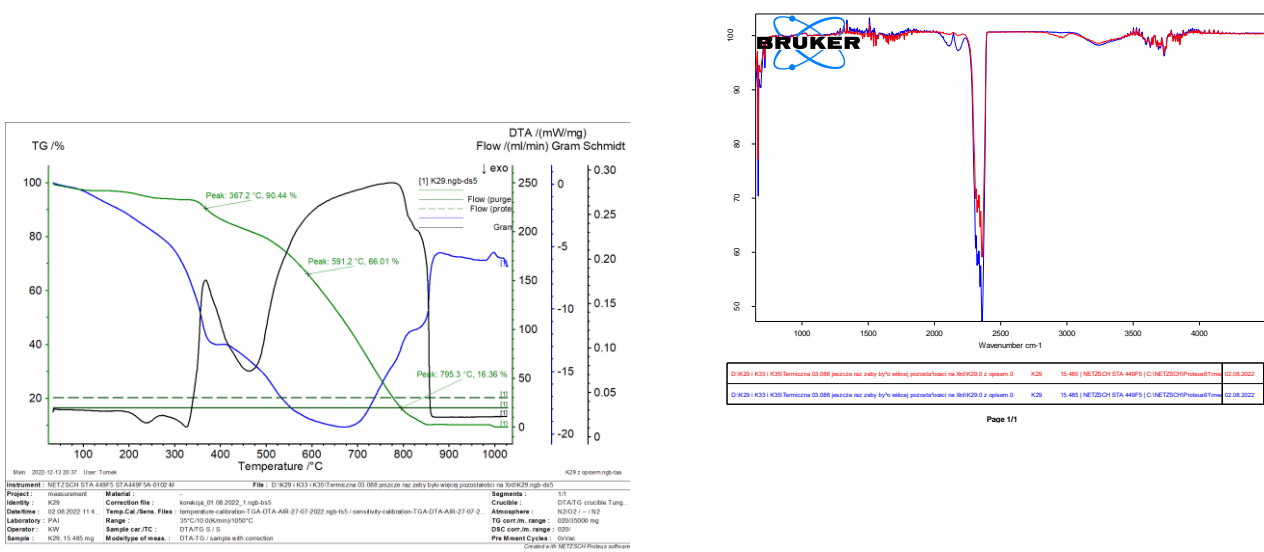


Figure 4. a) TG-DTA traces of K1 and **b)** IR spectra decomposition product

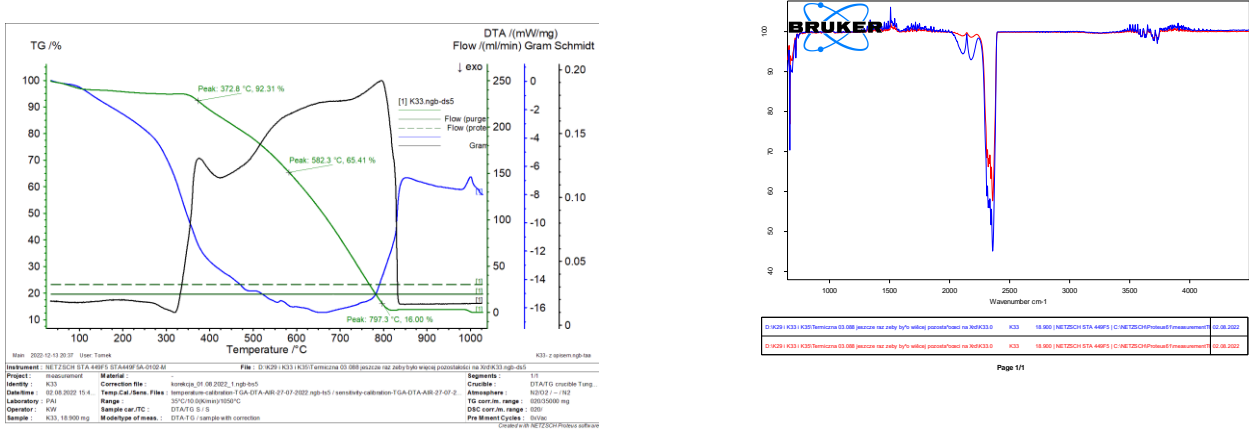


Figure S5. a) TG-DTA traces of K2 and **b)** IR spectra decomposition products.

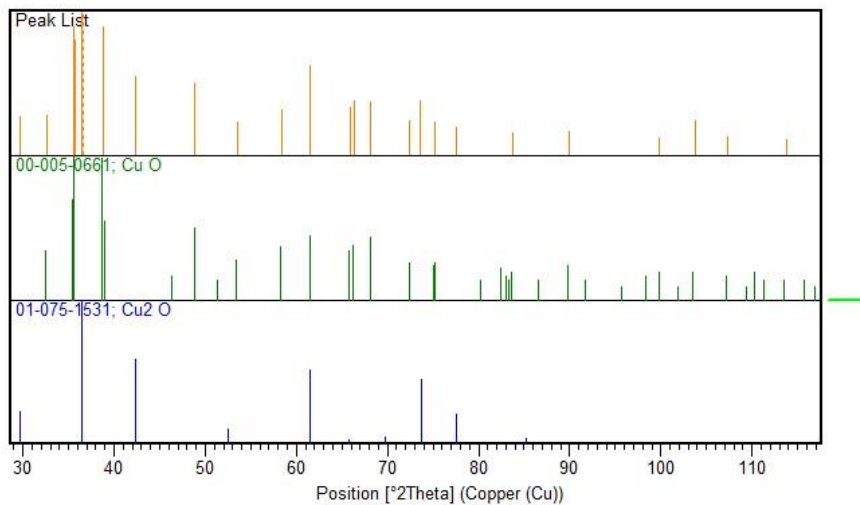


Figure S6. XRD of the thermal analysis residue of **K1**.

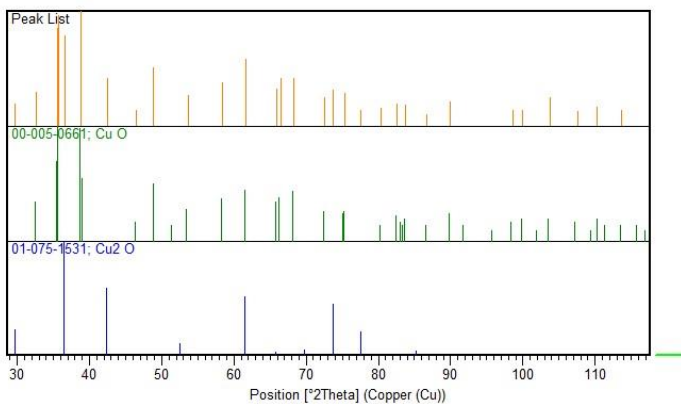


Figure S7. XRD of the thermal analysis residue of **K2**.

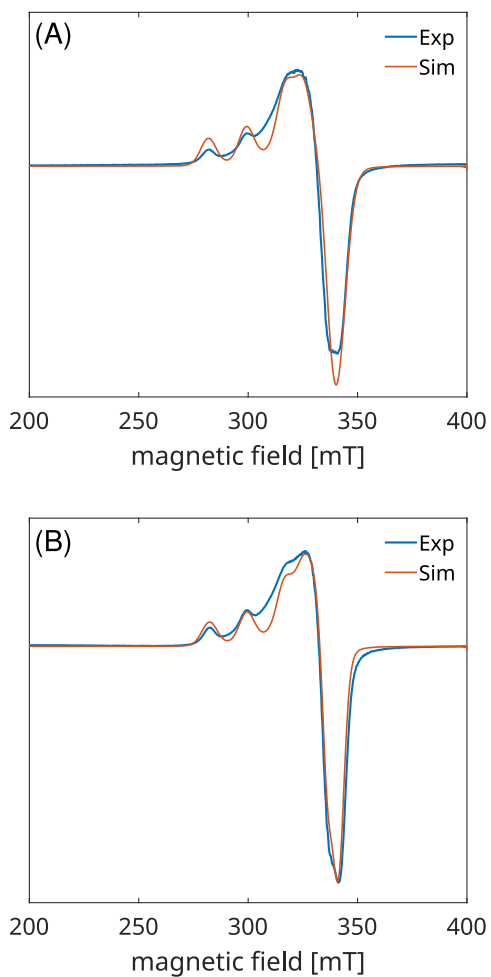


Figure S8. Powder EPR spectra recorded for **K1** (A) and **K2** (B) at 77 K.

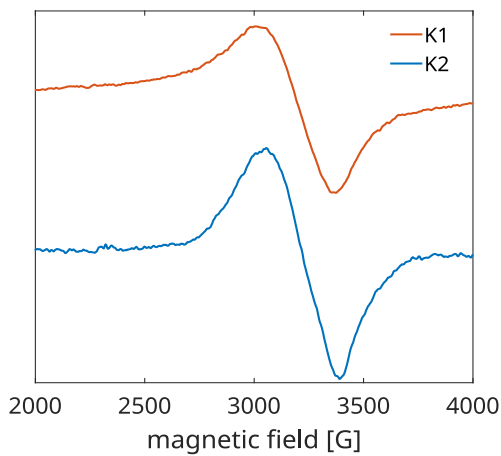


Figure S9. Powder EPR spectra recorded for **K1** and **K2** at 350 K.

Table S1. The theoretical values of the $J(Cu_1-Cu_2)$ magnetic coupling constants [cm^{-1}], estimated within the broken-symmetry and spin-flip approach with B3LYP functional and def2-SVP/def2-QZVPP(Cu) basis set according to the three schemes: spin-projected (SP), spin-unprojected (SUP) and approximate spin-projected (AP).

	K1	K2
Broken Symmetry/B3LYP/def2-SVP+def2-QZVPP for Cu		
E(High-Spin)-E(BrokenSym)	673.941 (antiferromagnetic)	693.172 (antiferromagnetic)
J(SP)	-673.94	-693.17
J(SUP)	-336.97	-346.59
J(AP)	-632.18	-649.28
Spin-Flip/B3LYP/def2-SVP+def2-QZVPP for Cu		
E(High-Spin)-E(BrokenSym)	674.353 (antiferromagnetic)	693.295 (antiferromagnetic)
J(SP)	-674.35	-693.29
J(SUP)	-337.18	-346.65
J(AP)	-632.58	-649.42

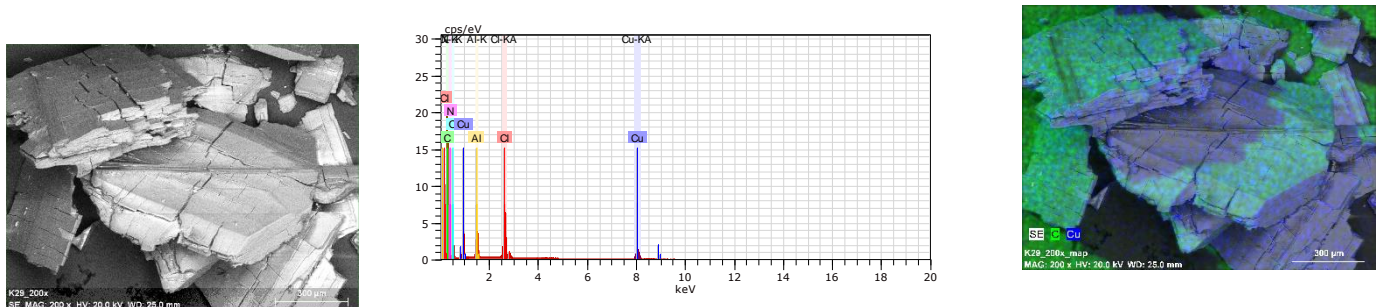


Figure S10. SEM/EDX images of K1 mapping scanning size 300 μm .

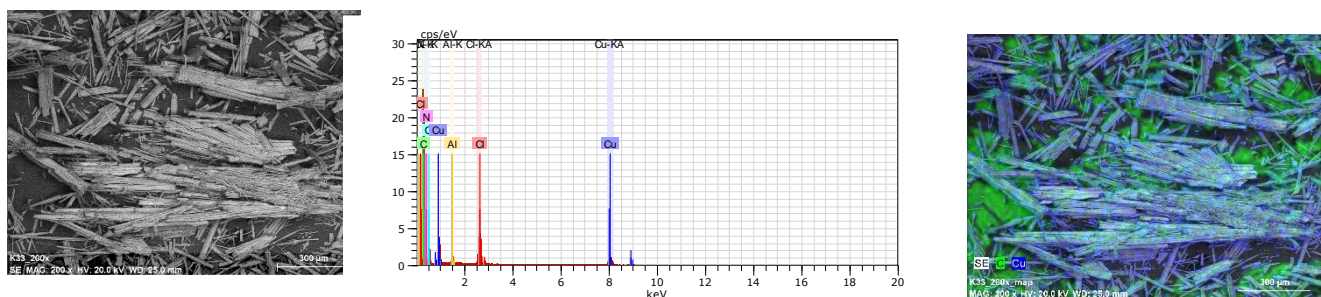


Figure S11. SEM/EDX images of K2 mapping scanning size 300 μm .

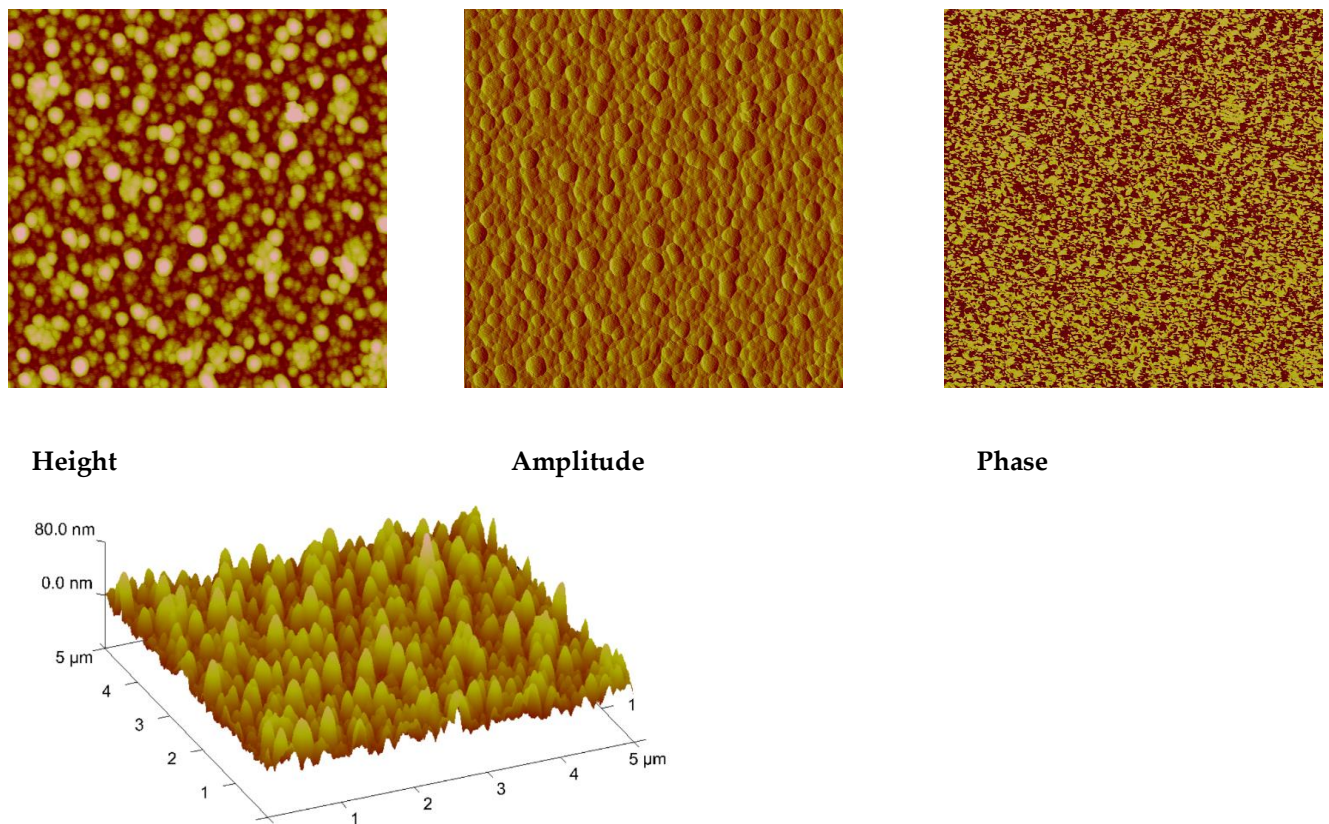


Figure S12. AFM of K1/Si, thermal deposition, scan size 5 μm , $R_a=4.02 \text{ nm}$, $R_q=5.36 \text{ nm}$.

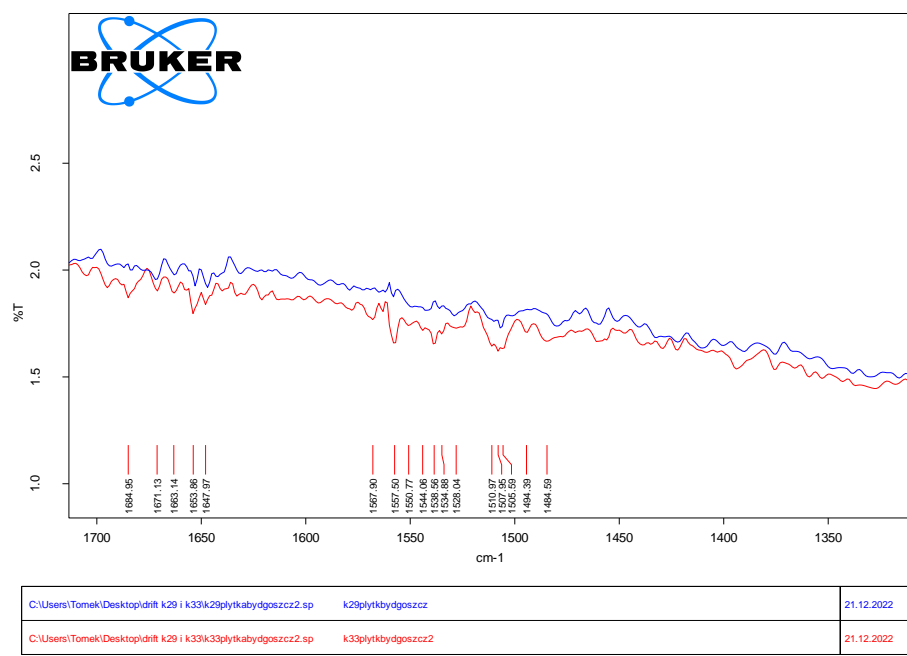


Figure 13. IR DRIFT of K1/Si and K2/Si materials- thermal vapour deposition.

Table S2. Relevant photophysical data of studied compounds: $\bar{\epsilon}_{\text{em}}$, $\bar{\epsilon}_{\text{ex}}$ [nm] Bp=8; λ [nm] (ε [$\text{dm}^3 \text{ mol}^{-1} \text{ cm}^{-1}$]); Stoke shift [nm], [cm^{-1}]; Q Bp=5.

Comp.	Solvent	λ_{ex} [nm]	λ_{em} [nm]	Fluoresc. Intensity a. u.	λ [nm] (ε [$\text{dm}^3 \text{ mol}^{-1} \text{ cm}^{-1}$])	A	Q	Stoke shift	
								[nm]	[cm^{-1}]
K1	acetone	409	1688725		402 (39628)	0,128	0,027	7	1428571
	methanol	412	1151660	388 (43963); 324 (46440) sh; 274 (104025)	0,142; 0,150; 0,336	0,013	24	416667	
	chloroform	350	398	201250	408 (37461); 324 (40248) sh; 272 (114861) 660 (13313)	0,121; 0,130; 0,371 0,043	0,0019	10	1000000
	DMSO	424	3021975	398 (44582); 290 (130960) sh	0,144; 0,423	0,017	26	384615	
K2	acetone	408	1315030		400 (40867)	0,132	0,035	8	1250000
	methanol	420	438415	388 (49845); 326 (50774) sh; 274 (123220)	0,161; 0,164; 0,398	0,011	32	312500	
	chloroform	392	260640	404 (43344); 328 (42724) sh; 272 (124458)	0,140; 0,138; 0,402	0,003	12	833333	
		350		664 (12384)	0,040				
	DMSO	424	1934125	394 (45201)	0,146	0,021	30	333333	
	acetonitrile	409	982115	392 (46749)	0,151	0,038	17	588235	

Table S3. Fluorescence data of the thin materials **K1/Si** and **K2/Si** – thermal vapour deposition.

Comp.	λ_{ex} [nm]	λ_{em} [nm]	Fluoresc. Intensity a. u.
K2	250	318	11715
		390	13580
		531	7320
	320	386	27980
		481	15870
		575	5050
K1	250	686	9145
		326	367045
		377	271315
	300	472	68955
		376	414115
		472	89570
	320	372	518885
		474	107320